Acta Oceanol. Sin., 2021, Vol. 40, No. 12, P. 114–124
https://doi.org/10.1007/s13131-021-1869-0
http://www.aosocean.com
E-mail: ocean2@hyxb.org.cn

Evolution and diagenetic implications of framboids in the methane-related carbonates of the northern Okinawa Trough

Kehong Yang[1]*, Zhimin Zhu[1], Yanhui Dong[1], Fengyou Chu[1], Weiyan Zhang[1]

[1] Key Laboratory of Submarine Geosciences, Second Institute of Oceanography, Ministry of Natural Resources, Hangzhou 310012, China

Received 2 April 2021; accepted 25 June 2021

Abstract

Authigenic carbonate samples were collected from the northern Okinawa Trough. Based on their carbon and oxygen isotopes, these samples were found to be methane-related carbonates precipitated by the anaerobic oxidation of methane (AOM). Petrological analysis revealed numerous framboidal pyrites that had been partly oxidized. In order to trace the variation and diagenetic information of these framboidal pyrites, their diameters and geochemical components were studied using an electron probe. The results showed that their diameters varied from 4 μm to 17 μm (n = 60; geometric mean of 9.9 μm) and were of a normal distribution. The diameters of single pyrite that formed the framboidal pyrites varied from 1 μm to 2 μm. The framboidal pyrites with diameters of 6–14 μm accounted for ~80% of the total. The geometric mean of 9.9 μm indicates that they are probably diagenetic pyrites that were precipitated in a lower dysoxic environment (weakly oxygenated bottom waters). The S/Fe ratio of the framboidal minerals ranged from 0 to 1.67, and the pyrite content of single framboid varied between 0% and 86.4%. Therefore, numerous pyrites were oxygenated to iron oxides or oxyhydroxides, and were retained as pseudomorphism pyrites. The size of framboidal pyrites precipitated in cold seeps can be used to trace the redox environment; however, acquisition of additional data via investigation of different cold seeps is necessary to obtain more persuasive results.

Key words: framboidal pyrite, grain size, S/Fe ratio, methane-related carbonate

Citation: Yang Kehong, Zhu Zhimin, Dong Yanhui, Chu Fengyou, Zhang Weiyan. 2021. Evolution and diagenetic implications of framboids in the methane-related carbonates of the northern Okinawa Trough. Acta Oceanologica Sinica, 40(12): 114–124, doi: 10.1007/s13131-021-1869-0

1 Introduction

In cold seep systems, the anaerobic oxidation of methane (AOM) in anoxic marine sediments is directly linked to sulfate reduction through a syntrophic interaction between methanogenic archaea and sulfate-reducing bacteria (e.g., Boetius et al., 2000; Orphan et al., 2001). This biogeochemical process is represented by the net reaction:

$$CH_4 + SO_4^{2-} \rightarrow HS^- + HCO_3^- + H_2O. \quad (1)$$

Authigenic pyrite, an important product of cold seeps, precipitates in anoxic environments when HS^- is integrated with free Fe in sediments and pore fluids (e.g., Chen et al., 2006; Peckmann et al., 2001; Pierre, 2017; Xie et al., 2013).

Authigenic pyrites in cold seeps have often been studied, particularly those in sediments (e.g., Crémière et al., 2020; Lin et al., 2016a, b, c, 2017; Peckmann et al., 2001; Pierre, 2017; Pirlet et al., 2012; Stakes et al., 1999; Xie et al., 2013; Zhang et al., 2014), and are mainly distributed in the sulfate-methane transition zone (SMTZ) (Lin et al., 2016a). Pyrites related to cold seeps mostly appear as aggregations with different morphologies, such as framboid, rod shape, and dumbbell-shaped; however, the framboidal form is predominant (Chen et al., 2006; Lin et al., 2017; Pierre, 2017; Stakes et al., 1999; Xie et al., 2013). Framboidal pyrites are densely packed, generally spherical aggregates of submicron-sized pyrite crystals (Rickard, 1970; Wilkin et al., 1996). Crystals composed of framboidal pyrites can be irregular, sub-euhedral, and euhedral. Euhedral pyrite without microcrystals can form as a result of the geochemical changes occurring during the crystallization evolution process (Merinero et al., 2008). Framboidal pyrites in methane-related carbonates always form in calcareous tests, for example, foraminiferal tests (e.g., Chen et al., 2007; Merinero et al., 2008; Stakes et al., 1999).

As mentioned, studies of authigenic pyrites in cold seeps have primarily focused on those in sediments, and have characterized the pyrite content, morphology, grain size, S and Fe isotopes, sediment environment, diagenesis, and formation mechanism. Integrated with the sulfur isotope of gypsum, the sulfur isotope sources of pyrites can be used to discuss the transition of a cold seep environment (Lin et al., 2016a; Pierre, 2017). Unlike the studies conducted on pyrites in sediments, studies of pyrites in methane-related carbonates fhave mainly focused on microscopic observations (Chen et al., 2006; Merinero et al., 2008; Peng et al., 2017), which may be attributable to the fact that they cannot be easily separated.

Framboid size-frequency distributions are widely used to determine the oxygenation states of paleo-waters (Wilkin et al., 1996). Framboid mean diameters can be used to help discriminate the oxygenation state of paleo-waters. However, a few conflicting findings reported in previous studies indicate that there is

Foundation item: The National Natural Science Foundation of China under contract Nos 41476050, 41106047, and 41506073.
*Corresponding author, E-mail: yangkh@sio.org.cn

always a finite chance that a particular framboid size-frequency distribution may be attributable to either syngenetic or diagenetic processes (Rickard, 2019) because the size-frequency dataset for framboids used to determine the oxygenation state of paleowater columns has been almost entirely reported by Wilkin et al. (1996). Therefore, more systematic framboid size-frequency measurements are warranted. The diameters of framboidal pyrites in cold seeps are lacking, and this aspect should be considered.

Framboidal pyrites are commonly found in the sediments or carbonates of cold seeps. Those in carbonates are always identified in biogenic tests, particularly foraminifera tests, which are relatively euxinic. However, the micro-environmental information and diagenetic processes indicated by framboidal pyrites in methane-related carbonates remain unclear. Therefore, this study aims to (1) characterize the framboidal pyrites in methane-related carbonate samples from the Okinawa Trough, and (2) determine the conditions under which they were formed based on their grain size and geochemical characteristics. Accordingly, this study describes the transformation of pyrite framboids into Fe oxides or oxyhydroxides.

2 Geological setting, sampling and methods

2.1 *Geological setting*

As part of the East China Sea, the Okinawa Trough is an extension bathyal basin of the Ryukyu trench-arc-basin tectonic system in the western Pacific continental margin (Sibuet et al., 1998; Fang et al., 2005; Luan and Qin, 2005). The Okinawa Trough extends ~1 200 km from Kyushu Island (Japan) in the northeast to the Ilan Plain (Taiwan Province, China) in the southwest (Fig. 1). The seafloor of the Okinawa Trough is divided into three parts according to its submarine geomorphic and geological characteristics, i.e., south, middle, and north sections, which are separated by the Miyako Strait and Tokara-kaikyo Strait.

Faults are common and earthquakes occur frequently in the Okinawa Trough (Luan and Qin, 2005). Volcanic and magmatic activities are also frequent (Luan and Qin, 2005). Sediments have a great diversity of sources (Pan and Shi, 1986). This area has favorable conditions for the formation of gas hydrates (Fang et al., 2003). Bottom-simulating reflectors (BSR), methane-related authigenic carbonates, and pyrites found in the Okinawa Trough have indicated the occurrence of gas hydrates (Peng et al., 2017; Sun et al., 2015; Lu et al., 2003; Tang et al., 2003; Wu et al., 2003).

2.2 *Sampling and methods*

Carbonate samples were collected using geological dredges during the survey of R/V *Kexue Yihao*, organized by the Institute of Oceanology, Chinese Academy of Sciences, during June 2013. The samples were collected at Site GT-D30 (29.520 0°N, 127.422 6°E, water depth of 256 m) on the western slope of the northern Okinawa Trough (Fig. 1). In this study, we investigate one car-

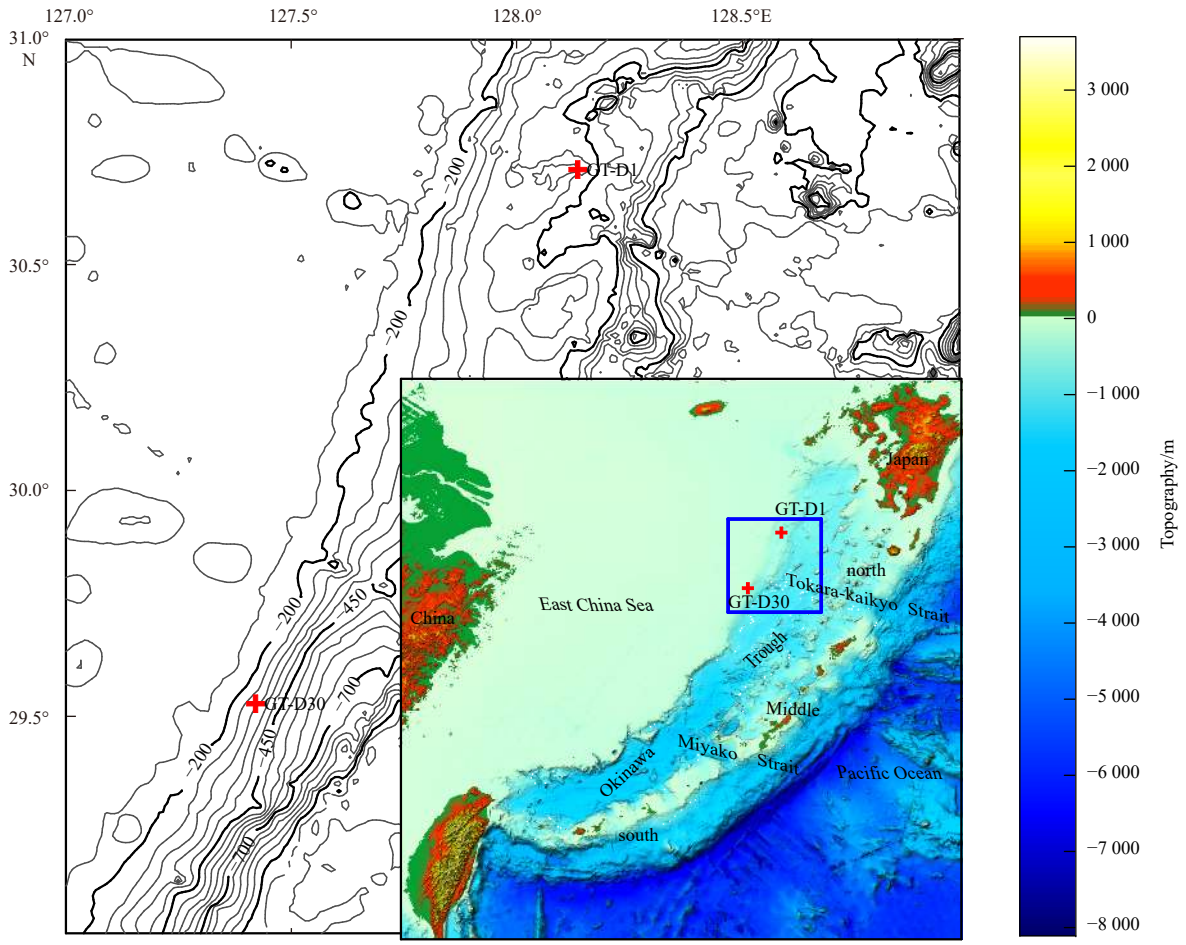

Fig. 1. Authigenic carbonate sampling locations. ETOPO1 data have been considered, which is a topography dataset available in resolutions of up to 1 min (https://www.ngdc.noaa.gov).

bonate sample collected from Site GT-D30, labeled as GT-D30-1 in Fig. 2, which had many biogenic marks.

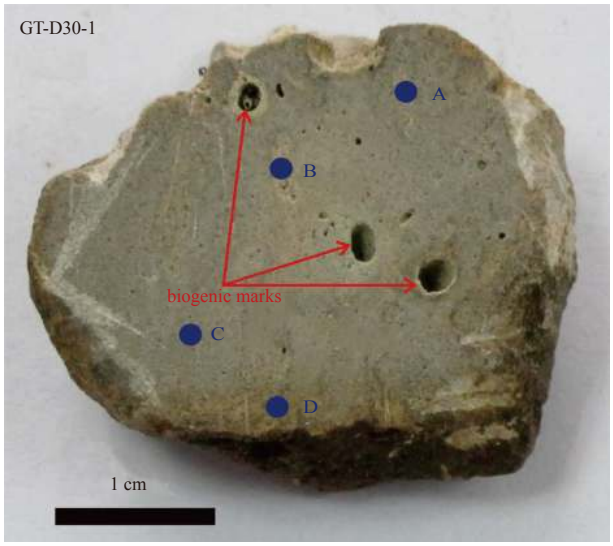

Fig. 2. Authigenic carbonate sample from Site GT-D30 investigated in this study (blue points and labels indicate the sampling locations for the C and O isotope analyses, and the biogenic marks are common).

The selected carbonates were cleaned with deionized water to remove residual sediment using ultrasonic waves. After cleaning, the selected carbonate sample was freeze-dried, cut into thin sections, and crushed to a <200 mesh powder using an agate mortar for X-ray diffraction (XRD) and carbon-oxygen isotope analyses.

Petrological observations, XRD, and electron microprobe analyses were conducted at the Key Laboratory of Submarine Geosciences, Ministry of Natural Resources. A Nikon polarizing microscope was used to observe mineralogical and petrological characteristics, and the mineralogical compositions of the samples were determined by XRD using an X'Pert Pro X-ray diffractometer with CuKα radiation. Oriented samples were scanned at intervals of 3°–70° (2θ) with a step size of 0.017° using a 45 kV accelerating voltage and 40 mA current.

Electron microprobe analyses were conducted to determine the Si, Sr, Ca, Ba, Al, Mg, Fe, Na, K, Mn, Ni, Cu, Ti, and S contents using the JXA-8100 electron microprobe equipped with an Oxford INCA X-sight energy-dispersive spectroscopy. Analyses were generally conducted using an accelerating voltage of 15 kV, a beam current of 20 nA, and a beam spot of 2 μm. The measured data were corrected following the ZAF method based on 53 standard minerals from SPI Company, USA.

Carbon and oxygen isotope ($\delta^{13}C$ and $\delta^{18}O$) analyses were conducted on bulk samples using the Finnigan MAT253 mass spectrometer at the State Key Laboratory of Marine Geology, Tongji University, Shanghai, China. The CO_2-generated reactions were conducted with ortho-phosphoric acid at 70°C. The precision was regularly checked using an international standard (NBS19), and the standard deviations were 0.07‰ for $\delta^{18}O$ and 0.04‰ for $\delta^{13}C$. The values were then converted to the international Vienna PeeDee Belemnite (V-PDB) scale using the NBS19 standard.

3 Results

The petrological observations indicated that the authigenic carbonate sample contained crypto-crystal structures (Fig. 3a), and numerous framboidal pyrites filled the calcareous tests (mainly foraminifera) (Fig. 3b). Single pyrites were composed of framboidal pyrites, some of which demonstrated shallow brassy and bright metallic luster, exhibiting marked pyrite characteristics, while some were yellow-white in color, exhibiting iron oxide characteristics.

The diameters of the framboidal pyrites in different tests (Fig. 4) ranged from 4 μm to 17 μm (geometric mean of 9.9 μm; n = 60) with a normal distribution (Fig. 5), while those of the single pyrites varied from 1 μm to 2 μm. Framboidal pyrites with diameters ranging from 6 μm to 14 μm accounted for approximately 80% of the total.

The mineral components included quartz, albite, chlorite, orthoclase, mica, high-Mg calcite, and dolomite (Fig. 6). The molar $MgCO_3$ percentage of calcite was calculated using the $d(104)$ peak value of calcite given in Å following the equation of Lumsden (1979):

$$MgCO_3\,(\mathrm{mol}\%) = 100 - (333.33d\,(104) - 911.99)\,. \qquad (2)$$

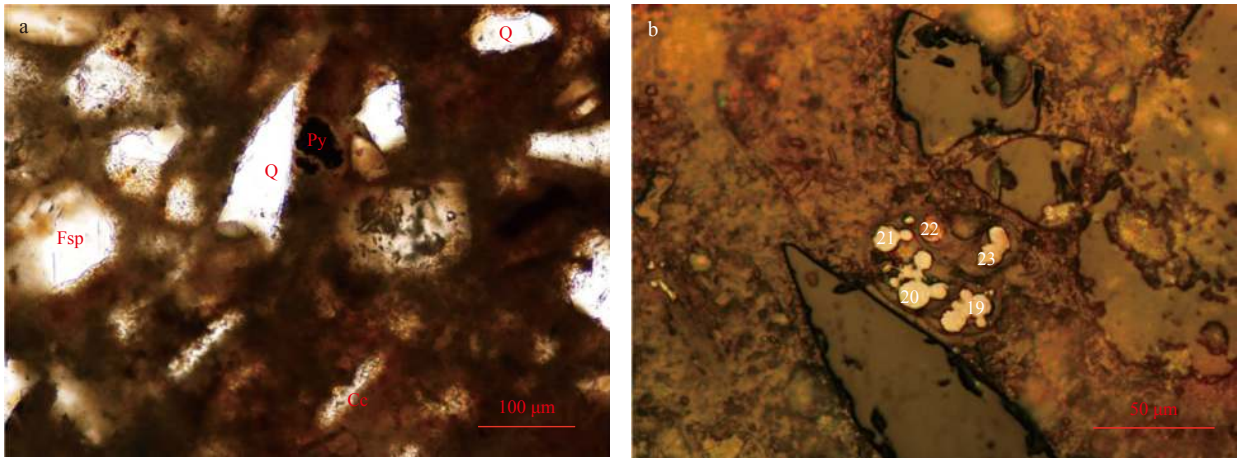

Fig. 3. Petrological characteristics of the authigenic carbonates from the Okinawa Trough. a. Plane-polarized light, b. reflected light. Q: quartz, Fsp: feldspar, Cc: calcite, and Py: pyrite. The numbers labeled in b are the same as in Fig. 4 which were analyzed using an electronic microprobe.

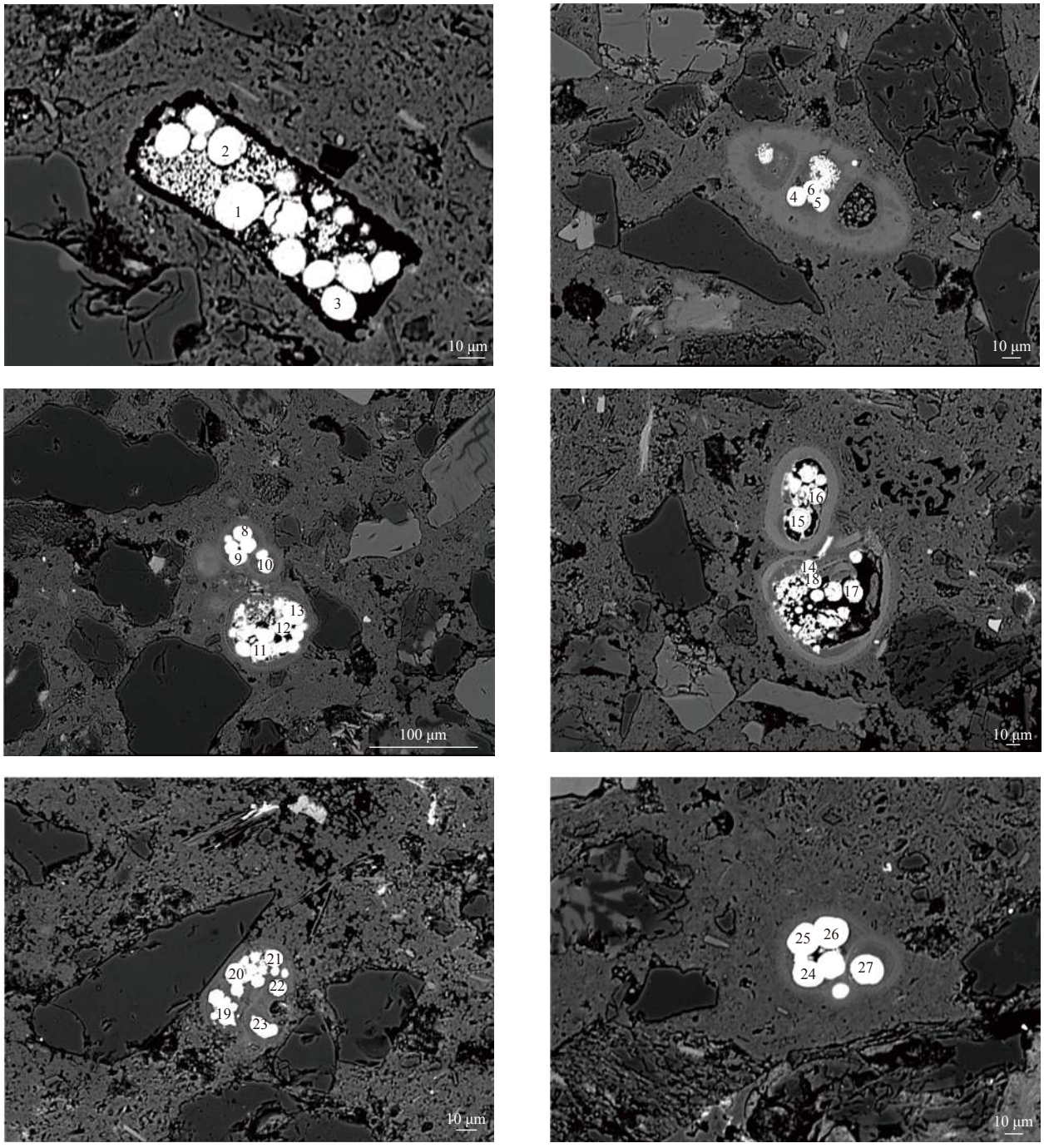

Fig. 4. Framboidal minerals analyzed using an electronic microprobe (labeled as numbers).

Calcite with a $MgCO_3$ content of < 5 mol% was considered as low-Mg calcite (LMC), while that with a $MgCO_3$ content of 5–20 mol% was referred to as high-Mg calcite (HMC) (Burton, 1993). Carbonate phases with >20 mol% $MgCO_3$ were classified as dolomite in this study.

The $\delta^{13}C$ and $\delta^{18}O$ values are presented in Table 1. The $\delta^{13}C$ value ranged between –53.7‰ and –52.6‰, with an average of –53.3‰ (V-PDB, n=4), while the $\delta^{18}O$ value ranged from 2.3‰ to 3.4‰, with an average of 2.7‰ (V-PDB, n = 4).

Electronic microprobe analyses were performed on some framboidal pyrites (Fig. 4). The component contents and S/Fe molar ratio values have been listed in Table 2. The S/Fe molar ratio of most framboid minerals was less than 1, and only the framboidal pyrites labeled as No. 22 presented with an S/Fe ratio of more than 1.

4 Discussion

4.1 *Formation environment of authigenic carbonates containing framboidal pyrites*

The carbon and oxygen isotopic results of our study showed that the authigenic carbonates from the Okinawa Trough were strongly depleted in $\delta^{13}C$ and enriched in $\delta^{18}O$, which is consistent with the data for AOM-generated authigenic carbonates

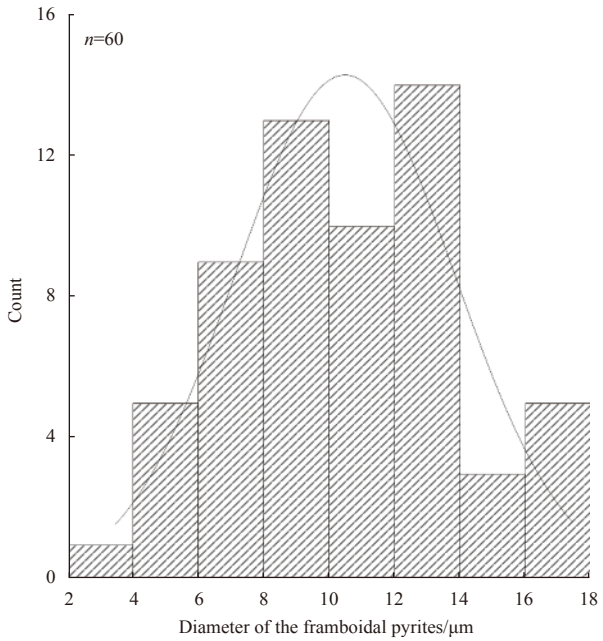

Fig. 5. Distribution histogram of the diameters of framboidal pyrites.

(Campbell, 2006; Suess, 2014). Therefore, the authigenic carbonates from the Okinawa Trough were the products of AOM. The $\delta^{13}C$ and $\delta^{18}O$ values reported in this study were at the endpoint, with relatively lower $\delta^{13}C$ values and higher $\delta^{18}O$ values than those reported in previous studies conducted in the Okinawa Trough (Fig. 7). The $\delta^{18}O$ and $\delta^{13}C$ values reported in the present study are similar to the results of the studies on carbonate crusts by Li et al. (2018) and Sun et al. (2019); however, the $\delta^{18}O$ contents were higher than those reported by Cao et al. (2020) and Sun et al. (2015). Cao et al. (2020) studied carbonate crusts precipitated on the seafloor, and Sun et al. (2015) studied carbonate chimneys formed by Fe-dependent AOM (Fe-AOM).

Sun et al. (2015) studied the chimney carbonate located at GT-D1 to the north of the sample location in this study (Fig. 1), and their $\delta^{56}Fe$ values, Fe oxide/oxyhydroxide contents, and negative correlation between the Fe and Ca contents indicated that Fe-AOM occurred during the formation of the chimney to a certain extent. Li et al. (2018) investigated authigenic carbonates obtained from the same location as described by Sun et al. (2015); their results indicated that the sulfate-dependent AOM (SR-AOM) and Fe-AOM both existed at different depths during carbonate precipitation, and that these two processes occurred in the SMTZ and underlying sulfate-depleted zone, respectively. Therefore, the carbonate precipitation environment in the studied area was complex, and SR-AOM and Fe-AOM might have occurred. The mineral components of the seep carbonates can also provide an important geological environment when they precipitated (e.g. Peckmann et al., 2001; Greinert et al., 2001; Naehr et al., 2007; Pierre et al., 2012). The conditions during the Mg-calcite precipitation significantly differed to those during aragonite formation. In cold seep environments, it is widely accepted that aragonite forms in environments with higher SO_4^{2-} and lower PO_4^{3-} levels; however, Mg-calcite precipitation is favored in high PO_4^{3-} and low SO_4^{2-} solutions (Greinert et al., 2001). Low sulfate levels are generally considered to promote dolomite precipitation (Baker and Kastner, 1981). Additionally, AOM increases the concentration of CO_3^{2-} through sulfate reduction, favoring dolomite formation (Moore et al., 2004). Generally, that the pore water geochemistry of methane seeps, particularly, the conditions at the SMTZ, which are characterized by pronounced microbial activity (i.e., SR-AOM), high pH, alkalinity and sulfide concentrations, and low sulfate concentrations, is suitable for dolomite

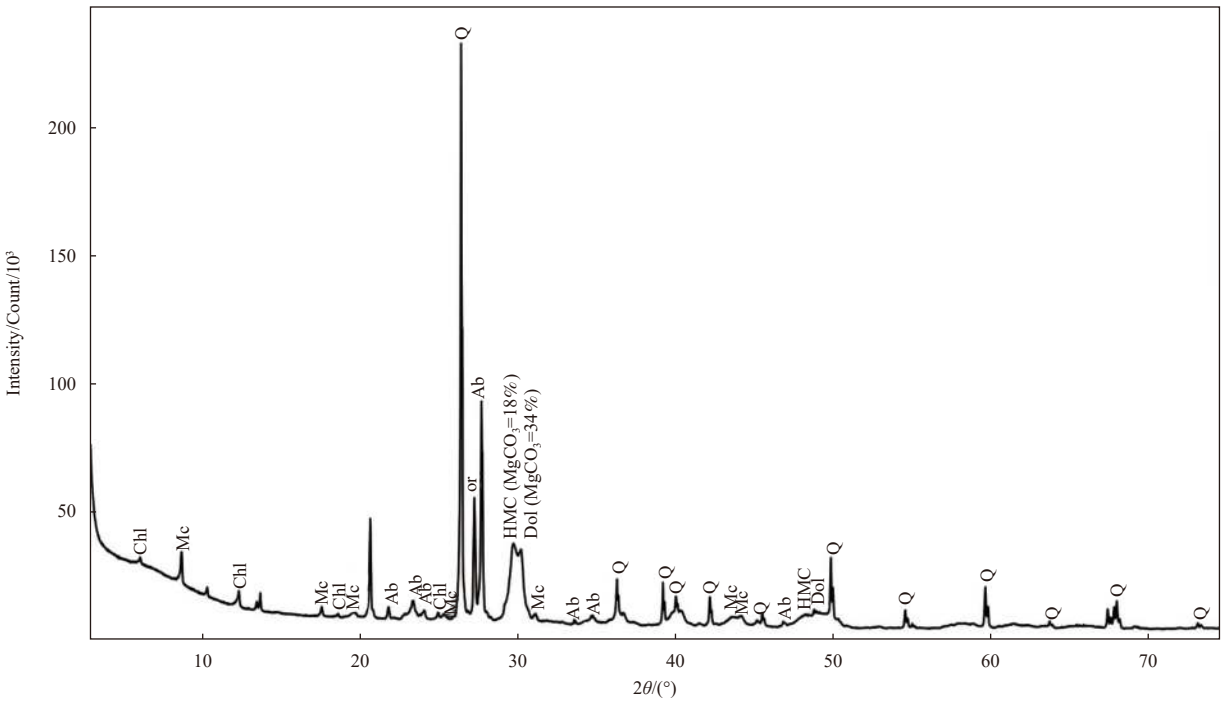

Fig. 6. Mineral compositions of the carbonate sample according to X-R diffraction analysis. Q: quartz, Chl: chlorite, Mc: mica, Ab: albite, Or: orthoclase, HMC: high-Mg calcite, and Dol: dolomite.

Table 1. $\delta^{13}C$ and $\delta^{18}O$ compositions of the methane-related carbonates from Site GT-D30 in the Okinawa Trough

Sample	Location	$\delta^{13}C$ (V-PDB)/‰	$\delta^{18}O$ (V-PDB)/‰
GT-D30-1	A	−53.7	2.3
GT-D30-1	B	−53.1	2.4
GT-D30-1	C	−53.6	3.4
GT-D30-1	D	−52.6	2.6

Table 2. Compositions of the samples measured using an electron microprobe and goethite

No.	SiO_2	CaO	Al_2O_3	MgO	Na_2O	K_2O	P_2O_5	FeO	S	α-FeO(OH)	FeS_2	S/Fe	Total
1	3.81	1.41	0.03	1.04	0.27	0.03	0.62	75.88	0.15	93.6	0.3	0.004	101.1
2	4.03	1.61	0.03	0.79	0.19	0.04	0.82	76.47	3.15	90.1	5.9	0.093	103.6
3	4.13	1.71	0.14	0.79	0.14	0.05	0.72	75.97	0.12	93.7	0.2	0.003	101.6
4	2.46	1.79	0.02	1.73	0.13	0.01	0.55	72.73	0.23	89.6	0.4	0.007	96.7
5	2.82	1.88	0.00	1.61	0.09	0.01	0.54	76.19	0.19	93.9	0.3	0.006	101.2
6	6.18	2.92	0.17	1.80	0.17	0.04	2.21	70.42	0.09	86.9	0.2	0.003	100.6
7	2.60	2.58	0.13	2.01	0.08	0.01	0.50	77.34	0.14	95.4	0.3	0.004	103.6
8	3.65	1.68	0.08	1.16	0.17	0.03	0.81	78.11	0.16	96.3	0.3	0.004	104.2
9	3.77	1.70	0.05	1.07	0.15	0.01	0.64	78.73	0.12	97.2	0.2	0.003	104.8
10	3.50	1.81	0.05	1.09	0.06	0.02	0.71	79.91	0.13	98.6	0.2	0.004	106.1
11	3.23	2.09	0.43	0.38	0.71	0.07	1.06	70.72	21.35	57.7	40.0	0.679	105.7
12	3.49	1.70	0.04	0.73	0.52	0.05	0.86	76.86	6.34	86.2	11.9	0.186	105.5
13	4.46	2.20	0.18	0.66	0.95	0.06	1.46	70.18	19.54	59.6	36.6	0.627	106.2
14	8.01	3.13	0.23	1.36	0.43	0.07	3.01	71.23	0.04	88.0	0.1	0.001	104.3
15	2.76	1.48	0.09	0.44	1.15	0.06	0.69	69.43	24.95	51.1	46.8	0.809	104.6
16	8.61	3.23	0.38	1.44	0.62	0.11	3.10	69.01	0.07	85.2	0.1	0.002	102.8
17	8.76	3.05	0.24	1.18	0.65	0.10	3.32	71.65	0.05	88.5	0.1	0.001	105.9
18	7.79	2.94	0.25	1.34	0.36	0.06	3.09	70.47	0.04	87.1	0.1	0.001	103.0
19	3.42	1.53	0.01	1.82	0.18	0.01	0.72	77.52	0.77	94.7	1.4	0.022	103.9
20	3.05	1.28	0.00	2.05	0.18	0.03	0.33	79.87	1.54	96.6	2.9	0.043	106.4
21	3.16	1.77	0.02	1.81	0.28	0.05	0.90	76.24	3.72	89.1	7.0	0.110	104.0
22	0.60	1.35	0.06	0.44	0.95	0.08	0.13	62.17	46.07	12.8	86.4	1.667	102.8
23	2.48	1.33	0.19	1.51	0.33	0.03	0.81	68.12	26.58	47.2	49.8	0.878	103.8
24	3.48	1.41	0.00	1.51	0.15	0.02	0.53	78.84	0.13	97.3	0.2	0.004	104.6
25	2.26	1.25	0.02	2.03	0.21	0.03	0.52	77.47	8.74	83.6	16.4	0.254	106.3
26	2.49	1.45	0.01	1.86	0.15	0.03	0.62	78.78	2.66	93.7	5.0	0.076	105.3
27	2.24	1.10	0.00	1.73	0.04	0.02	0.17	80.09	0.17	98.8	0.3	0.005	104.4

Note: α-FeO(OH) and pyrite (FeS_2) contents are calculated according to the atomic ratios of framboidal minerals. S/Fe represents the molar ratio, and the values in the other columns excluding those in the column titled No. represent percentage values for mass.

formation (Tong et al., 2019). Therefore, both HMC and dolomite indicate low SO_4^{2-} concentrations. Additionally, their presence in cold seeps indicates that the SR-AOM process occurs in deeper sediments (Lu et al., 2018). Information on the lipid biomarker inventory, combined with the carbonate mineral data reported by Guan et al. (2019), also indicated that most samples formed at greater depths within the sediment column (with one exception) in this area. The $\delta^{13}C$ and $\delta^{18}O$ values reported in this study considerably differed to those of the Fe-AOM carbonate chimneys studied by Sun et al. (2015). HMC and dolomite were identified as the main carbonate minerals in our sample (Fig. 6), and it contained small amounts of aragonite. Therefore, we inferred that it precipitated in a low-SO_4^{2-} environment in the deeper sediments where SR-AOM mainly occurred, followed by the occurrence of subsequent uplift, erosion, and exposure on the seafloor.

In cold seep environments where abundant seawater-derived sulfate is available, sulfide produced by sulfate reduction preferably reacts with dissolved Fe to precipitate iron sulfide minerals including amorphous iron monosulfide, greigite, and mackinawite, which can subsequently be transformed to pyrite (Smrzka et al., 2020). Additionally, some studies have shown that bacterial-mediated sulfate reduction fosters the precipitation of pyrite, rather than that of siderite (e.g., Franchi et al., 2017). Hence, we speculated that the sample was formed at the bottom of the SMTZ under conditions of a low SO_4^{2-} concentration, wherein SR-AOM occurred and was close to the region where the Fe-AOM mainly occurred. The Fe^{2+} originating from the Fe-AOM then migrated upwards with the seep fluids to exhibit reactions with the HS^- at the bottom of the SMTZ, leading to the precipitation of pyrites (Peng et al., 2017).

4.2 *Sedimentary environment indicated by framboidal pyrites*

Framboidal pyrite is a common mineral in reducing environments and has been precipitated in both modern and ancient sedimentary environments. Some studies have also demonstrated that dissolved oxygen is involved in the formation of pyrites (Nielsen and Shen, 2004; Wilkin et al., 1996). The size distribution of framboidal pyrites can indicate a redox environment, even when they are oxidized to Fe oxides or oxyhydroxides, thus presenting as pseudomorphism pyrites (Lüning et al., 2003; Wignall et al., 2005). The maximum and average sizes indicate the in-

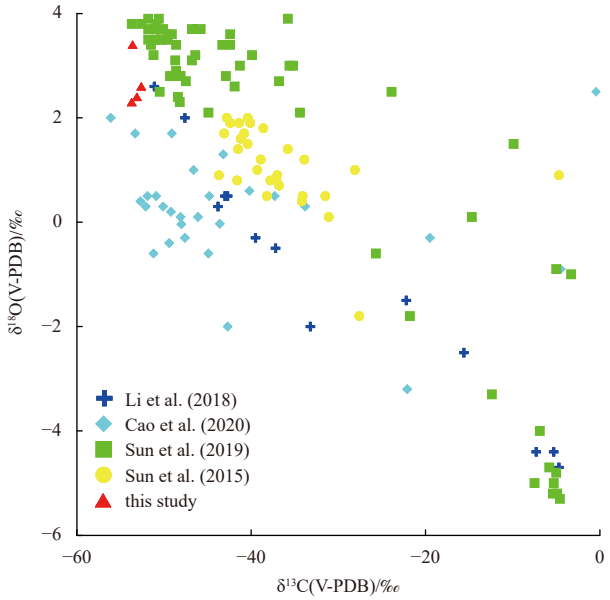

Fig. 7. $\delta^{13}C$ and $\delta^{18}O$ values of cold seep carbonates in the northern Okinawa Trough.

tensity of the redox environment (Wilkin and Barnes, 1997; Bond and Wignall, 2010). Under anoxic conditions (i.e., no oxygen in the bottom waters for a long period of time), the mean diameter of framboidal pyrites is 4–6 μm. Under lower dysoxic conditions (i.e., weakly oxygenated bottom waters), the mean diameter of framboidal pyrites varies from 6 μm to 10 μm, and exceeds 10 μm under upper dysoxic conditions (i.e., partial oxygen restriction in bottom waters) with a considerable proportion of pyrite being present as crystals. Nevertheless, some studies have pointed out that using the size-frequency of framboids to determine the oxygenation state of paleowater columns requires more data to support its use as a more robust identification tool (Rickard, 2019).

The framboidal minerals identified in this study were pyrites or Fe oxides and hydroxides (Table 2) with diameters of 4–17 μm and a geometric mean diameter of 9.9 μm. Although the diameter range of pyrite was large, 80% of the pyrite had diameters ranging from 6 μm to 14 μm. Therefore, the formation environment of the framboidal pyrites was relatively stable. According to Bond and Wignall (2010) and Wilkin et al. (1996), the geometric mean diameter implies that they precipitated under lower dysoxic conditions, which is consistent with the previous finding that lower dysoxic environments are common in cold seeps (Suess, 2014; Valentine, 2002). However, pyrite with a diameter less than 6 cm is also common in anoxic environments, and larger pyrites can also form under anoxic conditions or lower dysoxic condition; therefore, the finding that the pyrites precipitated under lower dysoxic conditions was robust. Pyrites, Fe oxides, and hydroxides filled the calcareous tests in our study. We also measured the framboidal pyrites of another study (Peng et al., 2017) that did not fill calcareous tests from sample Site GT-D1 following the same method, and they ranged from 5.4 μm to 15.4 μm in size (geometric mean diameter of 9.0 μm; n = 23). The geometric mean was similar to that of our sample (geometric mean diameter of 9.9 μm; n = 60), suggesting that they formed in similar environments. Hence, there were no notable differences between the diameters of the pyrites in and out of the calcareous tests in the cold seep carbonates, which mainly consisted of foraminifera with chamber sizes ranging from 50 μm to 1 000 μm that are much larger than framboidal pyrites. Therefore, the chamber size of calcareous tests does not generally limit the growth of framboidal pyrites during their formation and diagenesis.

Two types of framboidal pyrites with different formation paths exist in sediments: syngenetic pyrites formed in the water columns of modern euxinic environments, and diagenetic pyrites formed within the pore water of anoxic marine sediments underlying oxic water columns (Raiswell and Berner, 1985; Wilkin et al., 1996), which have different sizes, S isotope values, bulk rock C/S ratios, and degrees of mineralization (Lin et al., 2016b; Wilkin et al., 1996). Diagenetic pyrites are larger and demonstrate more variable sizes (Wilkin et al., 1996) and relatively higher $\delta^{34}S$ values; they are related to the SR-AOM (Lin et al., 2016b) and contain "excess" sulfide. Although consideration of the size frequency of framboids to determine their oxygenation state yields robust results, using the standard deviation value as a discriminator between syngenetic and diagenetic framboids is appropriate, as the geometric mean sizes of syngenetic and diagenetic framboids significantly differ, and the probability of framboids with a geometric mean diameter larger than 9.1 μm being syngenetic is less than or equal to 5% (Rickard, 2019). The geometric mean diameter of the framboids in the calcareous tests was 9.9 μm, while that of the framboids outside the tests was 9.0 μm; therefore, they were highly likely to be diagenetic framboids.

The pyrites derived from the Okinawa Trough were smaller than those derived from cold seeps worldwide (Table 3). Framboidal pyrites in the authigenic carbonates of the Nyegga pockmark and Black Sea were larger than those identified in this study. In the Nyegga pockmark, pyrite framboids in authigenic

Table 3. Sizes and characteristics of pyrites in cold seeps worldwide

Location	Size	Occurrence	References
Monterey Bay, California	5–20 μm	inside the chamber of foraminifera shells	Stakes et al. (1999)
Nyegga pockmark, Norwegian Sea	20–40 μm	in authigenic carbonates, throughout the micritic aragonite	Mazzini et al. (2006), Feng et al. (2015)
Black Sea	20–30 μm, formed of smaller globules of approximately 3–4 μm in diameter or smaller less	pyrite crusts in sediments	Peckmann et al. (2001)
Black Sea	–	in the authigenic carbonates	Mazzini et al. (2004),
Gulf of Cadiz (SW Iberian Peninsula)	5.5–59.1 μm, framboids with an average diameter of 21.3 μm	in the carbonates	Merinero et al. (2008)
Continental slope of the NE South China Sea	5–20 μm	authigenic pyrites in sediments	Zhang et al. (2014)
Shenhu area, South China Sea	2.3–132 μm with an varied average in different layers	pyrite aggregates in sediments	Lin et al. (2016a, b)
Okinawa Through	4–17 μm	in authigenic carbonates	this study

Note: – means no data.

carbonates were observed throughout micritic aragonite and they had precipitated in proximity of the seafloor during slow hydrocarbon seepage (Mazzini et al., 2006). The environment close to the seafloor is relatively more oxidized, and the precipitation of aragonite benefits from a high SO_4^{2-} concentration and alkalinity, and such aspects indicate the existence of partial oxidizing conditions. Therefore, the larger size of the framboidal pyrites from the Nyegga pockmark suggests a partially oxidized environment (upper dysoxic) in the pore water, which can cause the formation of pyrites with a broad range of sizes. In the Black Sea, Peckmann et al. (2001) found that framboidal pyrites formed in lacustrine sediments were not related to cold seeps. Therefore, the size of framboidal pyrites in cold seep carbonates can be used to robustly trace the changes of redox environments.

Table 3 also shows that there was no clear difference between the sizes of pyrites in most studies, excluding Lin et al. (2016b). Although the maximum diameter of pyrites from methane-rich sediments could reach 132 μm (Lin et al., 2016b), the mean diameter was 13.1 μm, and 75% of the framboidal pyrites had a diameter less than 15.5 μm. Therefore, larger pyrites may have been less common. However, regardless of the occurrence of precipitation in related methane seeps, all types of pyrites can be present in cold seeps. Therefore, when considering the size of framboidal pyrites present in cold seep carbonates to identify the environment under which they formed, whether their precipitation is related to cold seeps must be determined.

4.3 *Evolution characteristics of framboidal pyrites*

In an anoxic sulfidic environment, iron sulfides are linked to the activity of sulfate-reducing bacteria (Berner, 1984; Merinero et al., 2008), which reduce SO_4^{2-} and form pyrite (FeS_2) or iron sulfide (FeS), as expressed by Eqs (3) or (4) and Eq. (5):

$$SO_4^{2-} + Fe^{2+} + \text{organic matter} \rightarrow FeS_2 + HCO_3^-, \quad (3)$$

$$SO_4^{2-} + Fe^{2+} + \text{organic matter} \rightarrow FeS + HCO_3^-, \quad (4)$$

$$FeS + H_2O + O_2 \rightarrow FeS_2 + OH^-. \quad (5)$$

In cold seep environments, methane reacts with SO_4^{2-} through a syntrophic interaction between methanogenic archaea and sulfate-reducing bacteria (e.g., Boetius et al., 2000; Orphan et al., 2001), which is expressed in Eq. (1). Hydrogen sulfide can combine with iron and other elements retained in the walls and coatings of bacteria cells, favoring the precipitation of pyrite and other iron sulfides (Merinero et al., 2008).

The chemical compositions of the framboidal pyrites in the carbonates from the Okinawa Trough indicated that the S/Fe ratios of framboid minerals were less than 1, excluding framboidal mineral No. 22. Therefore, most framboids have low S contents. The S/Fe ratio indicated that only a few framboids were pyrite (such as framboidal No. 22). Many framboids were mainly composed of iron oxides or oxyhydroxides and presented as pseudomorphism pyrite, suggesting that they were oxidized from framboidal pyrites. The S/Fe ratios were consistent with the polarizing microscope observations. For example, framboid No. 22 exhibited clear pyrite characteristics under reflected light, such as a shallow brassy and bright metallic luster (Fig. 3b).

Different pyrite formation paths can result in differences in the size and S/Fe ratio. The difference in the S/Fe ratio in this study was not due to pyrite formation as the pyrites were oxidized to iron oxides or hydroxides. Pyrite oxides can exhibit the original framboid pseudomorphism after pyrite (Merinero et al., 2008), and pyrite oxidation studies have shown that pyrite first transforms into zomolnokite ($FeSO_4 \cdot H_2O$) before being oxidized to lepidocrocite (γ-FeO(OH)) and then goethite (α-FeO(OH) (Huggins et al., 1980; Merinero et al., 2008). Oxidized paths of pyrite have been observed in many cold seeps. For example, iron oxides have been found around the framboidal pyrites of the G11 pockmark in the Norwegian Sea (Mazzini et al., 2006), and framboidal pyrites oxidized to goethite have been observed in the carbonate chimney from the Gulf of Cadiz (Merinero et al., 2008).

The chemical components determined by the electronic probe (Table 2) indicated that the Si and Al contents were low; thus, the FeO in aluminum silicates can be ignored. Therefore, assuming that all of the S was present as pyrite (FeS_2) and the remaining Fe was present as goethite (α-FeO(OH)), we recalculated the pyrite and goethite contents of each framboid according to the electronic balance principle, and the recalculated results are listed in Table 2, which showed that the maximum pyrite content was 86.4% in all measured framboids, and 13 of the 27 framboids were goethite (its content larger than 90%). After recalculation, all of the total contents were approximately 100% with a range of 96.7%–106.4%, indicating that assuming the framboids are pyrite (FeS_2) and goethite (α-FeO(OH)) was reasonable. However, the total content of most framboids was larger than 100%, which could be due to the following reasons. First, we supposed that the oxidized product only contained goethite during recalculation; however, in a strongly oxidizing environment, pyrite can also be oxidized to magnetite and limonite (Wilkin and Barnes, 1997). Second, the S/Fe ratio of pyrite was not exactly 2:1 because of the formation path of pyrite, which first transforms into FeS, then Fe_3S_4, and finally to framboidal pyrites with the addition of S (Wilkin and Barnes, 1997).

4.4 *Diagenesis indicated by framboidal pyrites*

The optical microscopy observations and electronic probe results all indicated that the pyrite samples were likely diagenetic framboids, which coexisted with their oxidizing products (iron oxides or hydroxides) in the same calcareous test; therefore, both the pyrites and their oxidizing products formed after the precipitation of the calcareous test in the sediments. Following precipitation, the soft tissue was degraded, and pyrites precipitated then in the calcareous tests. Thus, the relationship between framboidal pyrites and organic matter (biofilm) in low-temperature diagenetic environments has been verified (Maclean et al., 2008).

Anoxic and oxic conditions are common in cold seeps (Birgel et al., 2011; Feng et al., 2009, 2013). The size of pyrites in our study varied from 6 μm to 17 μm, indicating lower dysoxic conditions (weakly oxygenated bottom waters). However, most pyrites were oxidized into iron oxides or hydroxides, such that the oxidation degree increased with the weakening (or even extinction) of the cold seep. The low S/Fe ratios indicated that the framboidal pyrites were highly oxidized, suggesting that oxidation was stronger after their formation. This may be due to the increase in oxidation during the uplift, erosion, and exposure of carbonate on the seafloor.

Some studies have demonstrated that pyrites can enrich trace elements in a diagenetic environment, including Au (Scott et al., 2009), Co, and As (Large et al., 1999). The electronic probe results indicated the presence of aluminosilicate minerals with varying contents (Table 2), which is consistent with the electron microprobe results of Merinero et al. (2008) and Cao et al. (2020), and can be interpreted as clay minerals and organic matter filling interstices in the framboids (Merinero et al., 2008). Therefore,

there were no obvious correlations between FeS_2 and Si, Ca, Al, K, and P (Table 4). While there was a strong positive correlation between FeS_2 and Na and a negative correlation between FeS_2 and Mg (Table 4). Mg^{2+} and Na^+ are common ions in the pore water of cold seeps (e.g., Snyder et al., 2007; Tsunogai et al., 1996; Wang et al., 2019; Xu et al., 2018), and the recrystallization of framboidal pyrites causes a decrease in the Mg content (Merinero et al., 2008). However, there is no explanation for the increase in the Na content with pyrite formation. Therefore, under the influence of cold seeps and the relatively closed environment in calcareous tests, the exchange of elements for the formation and oxidation of FeS_2 requires further study.

Table 4. Correlations between FeS_2 and major elements

	SiO_2	CaO	Al_2O_3	MgO	Na_2O	K_2O	P_2O_5
FeS_2	–0.418	–0.275	0.153	–0.536	0.722	0.335	–0.233

5 Conclusions

Framboidal pyrites in the carbonate sample from the Okinawa Trough were observed in calcareous tests and formed under the effect of the AOM. The framboidal pyrites ranged from 4 μm to 17 μm in size, with a geometric mean of 9.9 μm. According to the mean geometric diameter, the framboidal pyrites in the carbonate sample from the northern Okinawa Trough were highly likely to be diagenetic pyrites. Compared with the carbonate minerals, we speculate that these framboidal pyrites may precipitate under lower dysoxic conditions (weakly oxygenated bottom waters). Similar to the size of framboidal pyrites formed in other sediment environments, the size of the framboidal pyrites formed in cold seeps can also indicate the precipitation environment. Although this study provides useful findings, data from more cold seeps are required to obtain better results.

During the diagenesis of methane-related carbonates in the study area, framboidal pyrites were completely or partly oxidized into iron oxides or hydroxides, which retained the original framboidal pseudomorphism. The residual pyrites suggest that methane-carbonates experienced diagenesis. The electronic probe results demonstrated that the Mg content decreased during the oxidation of framboidal pyrites.

Acknowledgements

We are grateful to the crew and scientists of the *Kexue Yihao* cruise in June 2013 for sample collection. We thank Jihao Zhu at the Key Laboratory of Submarine Geosciences, Ministry of Natural Resources for the electron microprobe analyses, and Xiaoying Jiang at Tongji University for the carbon and oxygen isotope analyses.

References

Baker P A, Kastner M. 1981. Constraints on the formation of sedimentary dolomite. Science, 213(4504): 214–216, doi: 10.1126/science.213.4504.214

Berner R A. 1984. Sedimentary pyrite formation: An update. Geochimica et Cosmochimica Acta, 48(4): 605–615, doi: 10.1016/0016-7037(84)90089-9

Birgel D, Feng D, Roberts H H, et al. 2011. Changing redox conditions at cold seeps as revealed by authigenic carbonates from Alaminos Canyon, northern Gulf of Mexico. Chemical Geology, 285(1–4): 82–96, doi: 10.1016/j.chemgeo.2011.03.004

Boetius A, Ravenschlag K, Schubert C J, et al. 2000. A marine microbial consortium apparently mediating anaerobic oxidation of methane. Nature, 407(6804): 623–626, doi: 10.1038/35036572

Bond D P G, Wignall P B. 2010. Pyrite framboid study of marine Permian-Triassic boundary sections: A complex anoxic event and its relationship to contemporaneous mass extinction. GSA Bulletin, 122(7–8): 1265–1279, doi: 10.1130/B30042.1

Burton E A. 1993. Controls on marine carbonate cement mineralogy: review and reassessment. Chemical Geology, 105(1): 163–179, doi: 10.1016/0009-2541(93)90124-2

Campbell K A. 2006. Hydrocarbon seep and hydrothermal vent paleoenvironments and paleontology: Past developments and future research directions. Palaeogeography, Palaeoclimatology, Palaeoecology, 232(2–4): 362–407, doi: 10.1016/j.palaeo.2005.06.018

Cao Hong, Sun Zhilei, Wu Nengyou, et al. 2020. Mineralogical and geochemical records of seafloor cold seepage history in the northern Okinawa Trough, East China Sea. Deep Sea Research Part I: Oceanographic Research Papers, 155: 103165, doi: 10.1016/j.dsr.2019.103165

Chen Duofu, Feng Dong, Su Zheng, et al. 2006. Pyrite crystallization in seep carbonates at gas vent and hydrate site. Materials Science and Engineering: C, 26(4): 602–605, doi: 10.1016/j.msec.2005.08.037

Chen Yingfeng, Matsumoto R, Paull C K, et al. 2007. Methane-derived authigenic carbonates from the northern Gulf of Mexico--MD02 Cruise. Journal of Geochemical Exploration, 95(1–3): 1–15, doi: 10.1016/j.gexplo.2007.05.011

Crémière A, Pellerin A, Wing B A, et al. 2020. Multiple sulfur isotopes in methane seep carbonates track unsteady sulfur cycling during anaerobic methane oxidation. Earth and Planetary Science Letters, 532: 115994, doi: 10.1016/j.epsl.2019.115994

Fang Yinxia, Gao Jinyao, Li Mingbi, et al. 2005. Relation between gas hydrate and geologic structures in the Okinawa Trough. Marine Geology & Quaternary Geology (in Chinese), 25(1): 85–91

Fang Yinxia, Li Mingbi, Jin Xianglong, et al. 2003. Formation condition of gas hydrate in Okinawa Trough of the East China Sea. Bulletin of Science and Technology (in Chinese), 19(1): 1–5, doi: 10.3969/j.issn.1001-7119.2003.01.001

Feng Dong, Chen Duofu, Peckmann J. 2009. Rare earth elements in seep carbonates as tracers of variable redox conditions at ancient hydrocarbon seeps. Terra Nova, 21(1): 49–56, doi: 10.1111/j.1365-3121.2008.00855.x

Feng Dong, Lin Zhijia, Bian Youyan, et al. 2013. Rare earth elements of seep carbonates: Indication for redox variations and microbiological processes at modern seep sites. Journal of Asian Earth Sciences, 65: 27–33, doi: 10.1016/j.jseaes.2012.09.002

Feng Xiancui, Wang Wei, Wang Wenqian, et al. 2015. Methane-derived authigenic carbonates in Nyegga pockmarks, offshore Mid-Norway. Geochimica (in Chinese), 44(4): 348–359

Franchi F, Rovere M, Gamberi F, et al. 2017. Authigenic minerals from the Paola Ridge (southern Tyrrhenian Sea): Evidences of episodic methane seepage. Marine and Petroleum Geology, 86: 228–247, doi: 10.1016/j.marpetgeo.2017.05.031

Greinert J, Bohrmann G, Suess E. 2001. Gas hydrate-associated carbonates and methane-venting at Hydrate Ridge: classification, distribution, and origin of authigenic lithologies. In: Paull C K, Dillon W P, eds. Natural Gas Hydrates: Occurrence, Distribution, and Detection. Washington, DC, USA: American Geophysical Union, 124: 99–113, doi: 10.1029/GM124p0099

Guan Hongxiang, Sun Zhilei, Mao Shengyi, et al. 2019. Authigenic carbonate formation revealed by lipid biomarker inventory at hydrocarbon seeps: A case study from the Okinawa Trough. Marine and Petroleum Geology, 101: 502–511, doi: 10.1016/j.marpetgeo.2018.12.028

Huggins F E, Huffman G P, Kosmack D A, et al. 1980. Mossbauer detection of goethite (α-FeOOH) in coal and its potential as an indicator of coal oxidation. International Journal of Coal Geology, 1(1): 75–81, doi: 10.1016/0166-5162(80)90007-5

Large D J, Sawłowicz Z, Spratt J. 1999. A cobaltite-framboidal pyrite association from the Kupferschiefer: possible implications for trace element behaviour during the earliest stages of diagenesis. Mineralogical Magazine, 63(3): 353–361, doi: 10.1180/002646199548574

Li Jiwei, Peng Xiaotong, Bai Shijie, et al. 2018. Biogeochemical processes controlling authigenic carbonate formation within the sediment column from the Okinawa Trough. Geochimica et Cosmochimica Acta, 222: 363–382, doi: 10.1016/j.gca.2017.10.029

Lin Zhizhong, Sun Xiaoming, Lu Yang, et al. 2016a. Stable isotope patterns of coexisting pyrite and gypsum indicating variable methane flow at a seep site of the Shenhu area, South China Sea. Journal of Asian Earth Sciences, 123: 213–223, doi: 10.1016/j.jseaes.2016.04.007

Lin Zhizhong, Sun Xiaoming, Lu Yang, et al. 2017. The enrichment of heavy iron isotopes in authigenic pyrite as a possible indicator of sulfate-driven anaerobic oxidation of methane: Insights from the South China Sea. Chemical Geology, 449: 15–29, doi: 10.1016/j.chemgeo.2016.11.032

Lin Zhizhong, Sun Xiaoming, Peckmann J, et al. 2016b. How sulfate-driven anaerobic oxidation of methane affects the sulfur isotopic composition of pyrite: A SIMS study from the South China Sea. Chemical Geology, 440: 26–41, doi: 10.1016/j.chemgeo.2016.07.007

Lin Qi, Wang Jiasheng, Algeo T J, et al. 2016c. Enhanced framboidal pyrite formation related to anaerobic oxidation of methane in the sulfate-methane transition zone of the northern South China Sea. Marine Geology, 379: 100–108, doi: 10.1016/j.margeo.2016.05.016

Lu Zhenquan, Gong Jianming, Wu Bihao, et al. 2003. Geochemical perspective of gas hydrate in the East China Sea. Marine Geology & Quaternary Geology (in Chinese), 23(3): 77–81

Lu Yang, Sun Xiaoming, Xu Huifang, et al. 2018. Formation of dolomite catalyzed by sulfate-driven anaerobic oxidation of methane: Mineralogical and geochemical evidence from the northern South China Sea. American Mineralogist, 103(5): 720–734, doi: 10.2138/am-2018-6226

Luan Xiwu, Qin Yunshan. 2005. Discovery of the cold seeps in the west Miyako section of Okiniwa Through. Chinese Science Bulletin (in Chinese), 50(8): 802–810

Lumsden D N. 1979. Discrepancy between thin-section and X-ray estimates of dolomite in limestone. Journal of Sedimentary Research, 49(2): 429–435

Lüning S, Kolonic S, Loydell D K, et al. 2003. Reconstruction of the original organic richness in weathered Silurian shale outcrops (Murzuq and Kufra basins, southern Libya). GeoArabia, 8: 299–308

Maclean L C W, Tyliszczak T, Gilbert P U P A, et al. 2008. A high-resolution chemical and structural study of framboidal pyrite formed within a low-temperature bacterial biofilm. Geobiology, 6(5): 471–480, doi: 10.1111/j.1472-4669.2008.00174.x

Mazzini A, Ivanov M K, Parnell J, et al. 2004. Methane-related authigenic carbonates from the Black Sea: geochemical characterisation and relation to seeping fluids. Marine Geology, 212(1–4): 153–181, doi: 10.1016/j.margeo.2004.08.001

Mazzini A, Svensen H, Hovland M, et al. 2006. Comparison and implications from strikingly different authigenic carbonates in a Nyegga complex pockmark, G11, Norwegian Sea. Marine Geology, 231(1–4): 89–102, doi: 10.1016/j.margeo.2006.05.012

Merinero R, Lunar R, Martínez-Frías J, et al. 2008. Iron oxyhydroxide and sulphide mineralization in hydrocarbon seep-related carbonate submarine chimneys, Gulf of Cadiz (SW Iberian Peninsula). Marine and Petroleum Geology, 25(8): 706–713, doi: 10.1016/j.marpetgeo.2008.03.005

Moore T S, Murray R W, Kurtz A C, et al. 2004. Anaerobic methane oxidation and the formation of dolomite. Earth and Planetary Science Letters, 229(1–2): 141–154, doi: 10.1016/j.epsl.2004.10.015

Naehr T H, Eichhubl P, Orphan V J, et al. 2007. Authigenic carbonate formation at hydrocarbon seeps in continental margin sediments: A comparative study. Deep Sea Research Part II: Topical Studies in Oceanography, 54(11–13): 1268–1291, doi: 10.1016/j.dsr2.2007.04.010

Nielsen J K, Shen Yanan. 2004. Evidence for sulfidic deep water during the Late Permian in the East Greenland Basin. Geology, 32(12): 1037–1040, doi: 10.1130/G20987.1

Orphan V J, House C H, Hinrichs K U, et al. 2001. Methane-consuming archaea revealed by directly coupled isotopic and phylogenetic analysis. Science, 293(5529): 484–487, doi: 10.1126/science.1061338

Pan Zhiliang, Shi Siqi. 1986. Study on sediments and sedimentation in Okinawa Trough. Marine Geology & Quaternary Geology (in Chinese), 6(1): 17–29

Peckmann J, Reimer A, Luth U, et al. 2001. Methane-derived carbonates and authigenic pyrite from the northwestern Black Sea. Marine Geology, 177(1–2): 129–150, doi: 10.1016/s0025-3227(01)00128-1

Peng Xiaotong, Guo Zixiao, Chen Shun, et al. 2017. Formation of carbonate pipes in the northern Okinawa Trough linked to strong sulfate exhaustion and iron supply. Geochimica et Cosmochimica Acta, 205: 1–13, doi: 10.1016/j.gca.2017.02.010

Pierre C. 2017. Origin of the authigenic gypsum and pyrite from active methane seeps of the southwest African Margin. Chemical Geology, 449: 158–164, doi: 10.1016/j.chemgeo.2016.11.005

Pierre C, Blanc-Valleron M M, Demange J, et al. 2012. Authigenic carbonates from active methane seeps offshore southwest Africa. Geo-Marine Letters, 32(5): 501–513, doi: 10.1007/s00367-012-0295-x

Pirlet H, Wehrmann L M, Foubert A, et al. 2012. Unique authigenic mineral assemblages reveal different diagenetic histories in two neighbouring cold-water coral mounds on Pen Duick Escarpment, Gulf of Cadiz. Sedimentology, 59(2): 578–604, doi: 10.1111/j.1365-3091.2011.01267.x

Raiswell R, Berner R A. 1985. Pyrite formation in euxinic and semi-euxinic sediments. American Journal of Science, 285(8): 710–724, doi: 10.2475/ajs.285.8.710

Rickard D T. 1970. The origin of framboids. Lithos, 3(3): 269–293, doi: 10.1016/0024-4937(70)90079-4

Rickard D. 2019. Sedimentary pyrite framboid size-frequency distributions: A meta-analysis. Palaeogeography, Palaeoclimatology, Palaeoecology, 522: 62–75, doi: 10.1016/j.palaeo.2019.03.010

Scott R J, Meffre S, Woodhead J, et al. 2009. Development of framboidal pyrite during diagenesis, low-grade regional metamorphism, and hydrothermal alteration. Economic Geology, 104(8): 1143–1168, doi: 10.2113/gsecongeo.104.8.1143

Sibuet J C, Deffontaines B, Hsu S K, et al. 1998. Okinawa trough back-arc basin: Early tectonic and magmatic evolution. Journal of Geophysical Research: Solid Earth, 103(B12): 30245–30267, doi: 10.1029/98jb01823

Smrzka D, Feng D, Himmler T, et al. 2020. Trace elements in methane-seep carbonates: Potentials, limitations, and perspectives. Earth-Science Reviews, 208: 103263, doi: 10.1016/j.earscirev.2020.103263

Snyder G T, Hiruta A, Matsumoto R, et al. 2007. Pore water profiles and authigenic mineralization in shallow marine sediments above the methane-charged system on Umitaka Spur, Japan Sea. Deep Sea Research Part II: Topical Studies in Oceanography, 54(11–13): 1216–1239, doi: 10.1016/j.dsr2.2007.04.001

Stakes D S, Orange D, Paduan J B, et al. 1999. Cold-seeps and authigenic carbonate formation in Monterey Bay, California. Marine Geology, 159(1–4): 93–109, doi: 10.1016/s0025-3227(98)00200-x

Suess E. 2014. Marine cold seeps and their manifestations: geological control, biogeochemical criteria and environmental conditions. International Journal of Earth Sciences, 103(7): 1889–1916, doi: 10.1007/s00531-014-1010-0

Sun Zhilei, Wei Hehong, Zhang Xunhua, et al. 2015. A unique Fe-rich carbonate chimney associated with cold seeps in the Northern Okinawa Trough, East China Sea. Deep Sea Research Part I: Oceanographic Research Papers, 95: 37–53, doi: 10.1016/j.dsr.2014.10.005

Sun Zhilei, Wu Nengyou, Cao Hong, et al. 2019. Hydrothermal metal

supplies enhance the benthic methane filter in oceans: An example from the Okinawa Trough. Chemical Geology, 525: 190–209, doi: 10.1016/j.chemgeo.2019.07.025

Tang Yong, Jin Xianglong, Fang Yinxia, et al. 2003. Seismic study of gas hydrate BSR in the Okinawa Trough. Acta Oceanologica Sinica (in Chinese), 25(4): 59–66, doi: 10.3321/j.issn:0253-4193.2003.04.008

Tong Hongpeng, Feng Dong, Peckmann J, et al. 2019. Environments favoring dolomite formation at cold seeps: A case study from the Gulf of Mexico. Chemical Geology, 518: 9–18, doi: 10.1016/j.chemgeo.2019.04.016

Tsunogai U, Ishibashi J, Wakita H, et al. 1996. Fresh water seepage and pore water recycling on the seafloor: Sagami Trough subduction zone, Japan. Earth and Planetary Science Letters, 138(1–4): 157–168, doi: 10.1016/0012-821X(95)00228-5

Valentine D L. 2002. Biogeochemistry and microbial ecology of methane oxidation in anoxic environments: a review. Antonie Van Leeuwenhoek, 81(1–4): 271–282, doi: 10.1023/A:1020587206351

Wang Meng, Li Qing, Cai Feng, et al. 2019. Formation of authigenic carbonates at a methane seep site in the middle Okinawa Trough, East China Sea. Journal of Asian Earth Sciences, 185: 104028, doi: 10.1016/j.jseaes.2019.104028

Wignall P B, Newton R, Brookfield M E. 2005. Pyrite framboid evidence for oxygen-poor deposition during the Permian-Triassic crisis in Kashmir. Palaeogeography, Palaeoclimatology, Palaeoecology, 216(3–4): 183–188, doi: 10.1016/j.palaeo.2004.10.009

Wilkin R T, Barnes H L. 1997. Formation processes of framboidal pyrite. Geochimica et Cosmochimica Acta, 61(2): 323–339, doi: 10.1016/S0016-7037(96)00320-1

Wilkin R T, Barnes H L, Brantley S L. 1996. The size distribution of framboidal pyrite in modern sediments: An indicator of redox conditions. Geochimica et Cosmochimica Acta, 60(20): 3897–3912, doi: 10.1016/0016-7037(96)00209-8

Wu Bihao, Zhang Guangxue, Zhu Youhai, et al. 2003. Progress of gas hydrate investigation in China offshore. Earth Science Frontiers (in Chinese), 10(1): 177–189, doi: 10.3321/j.issn:1005-2321.2003.01.021

Xie Lei, Wang Jiasheng, Wu Nengyou, et al. 2013. Characteristics of authigenic pyrites in shallow core sediments in the Shenhu area of the northern South China Sea: Implications for a possible mud volcano environment. Science China Earth Sciences, 56(4): 541–548, doi: 10.1007/s11430-012-4511-3

Xu Cuiling, Wu Nengyou, Sun Zhilei, et al. 2018. Methane seepage inferred from pore water geochemistry in shallow sediments in the western slope of the Mid-Okinawa Trough. Marine and Petroleum Geology, 98: 306–315, doi: 10.1016/j.marpetgeo.2018.08.021

Zhang Mei, Konishi H, Xu Huifang, et al. 2014. Morphology and formation mechanism of pyrite induced by the anaerobic oxidation of methane from the continental slope of the NE South China Sea. Journal of Asian Earth Sciences, 92: 293–301, doi: 10.1016/j.jseaes.2014.05.004